Identification of Selected Persistent Organic Pollutants in Agricultural Land by Carbon Nitride (C$_3$N$_5$) Based Nano Sensors

Puspamitra Panigrahi, Anuroop PS, Hoonkyung Lee, Hyeonhu Bae,
Thanayut Kaewmaraya, Ravindra Pandey, Tanveer Hussain,* and Akshaya Panigrahi*

Efficient detection of selected persistent organic pollutants (POPs) is extremely important for the safety of humans and for the moderation of agriculture. This calls for the design of versatile nanosensors capable of sensing toxic POPs with high sensitivity and selectivity. Inspired by this, the sensing characteristics of carbon nitride (C$_3$N$_5$) monolayers toward selected POPs are reported, such as Dichlorodiphenyltrichloroethane (DDT), Methoxychlor (DMDT), Fenthion (FT), Fenitrothion (FNT), and Rennol (RL), employing density functional theory calculations. Analysis of results predicts adsorption energies of −0.93, −1.55, −1.44, −0.98, and −1.15 eV for DDT, DMDT, FT, FNT, and RM, respectively, on C$_3$N$_5$ monolayers. Significant charge transfers among organic pollutants and C$_3$N$_5$ lead to distinct electronic properties of the conjugated complexes, revealed by the density of states, electrostatic potential, and work function calculations. To detect the selected pollutants in high humidity, the effects due to aqueous medium are considered. Additionally, a statistical thermodynamic analysis utilizing the Langmuir adsorption model is utilized to explore the influence of temperature and pressure.

1. Introduction

Persistent organic pollutants (POPs) are a class of toxic chemicals that can survive in the environment for several years before actual degradation. These POPs are also lipophilic and accumulate in the fatty tissue of living animals and humans, causing acute toxic effects.[1] The United Nations Environment Programme (UNEP) has identified a group of POPs, which are mostly pesticides, prohibited from being used for agricultural purposes.[2–4] However, there is still improper use of POPs with the disposal of various agrochemicals and industrial chemicals, which negatively affect humans, plant and animal species, as well as our natural ecosystems. The most commonly used POPs in agriculture are Dichlorodiphenyl-trichloroethane (DDT/C$_{14}$H$_9$Cl$_5$), Methoxy-chlor (DMDT/C$_{16}$H$_{15}$Cl$_3$O$_2$), Fenthion

P. Panigrahi
Centre for Clean Energy and Nano Convergence
Hindustan Institute of Technology and Science
Chennai 603103, India
E-mail: puspamitrap@hindustanuniv.ac.in

A. PS, A. Panigrahi
Central Institute of Brackishwater Aquaculture (ICAR-CIBA)
75 Santhome High Road, Chennai, Tamilnadu 600028, India

H. Lee
Department of Physics
Konkuk University
Seoul 05029, Republic of Korea

H. Bae
Department of Condensed Matter Physics
Weizmann Institute of Science
Rehovot 7610001, Israel

T. Kaewmaraya
Integrated Nanotechnology Research Centre, Department of Physics
Khon Kaen University
Khon Kaen 40002, Thailand

T. Kaewmaraya
Institute of Nanomaterials Research and Innovation for Energy (IN-RIE),
NANOTEC-KKU RNN on Nanomaterials Research and Innovation for Energy
Khon Kaen University
Khon Kaen 40002, Thailand

R. Pandey
Michigan Technological University
Michigan, MI 49931, USA

T. Hussain
School of Science and Technology
University of New England
Armidale, New South Wales 2351, Australia
E-mail: tanveer.hussain@une.edu.au

$(FT/C_{10}H_{15}O_3S_2P_1)$, Fenitrothion $(FNT/C_9H_{12}N_1O_5P_1S_1)$, and Rennol $(RL/C_8H_8Cl_4O_3S_1P_1)$, which are identified to be toxic to all living beings.

Among the mentioned POPs, DDT is commonly used as an insecticide in agriculture and is a human carcinogen. High exposure to DDT can cause vomiting, tremors or shakiness, and seizures and can also affect the liver and reproduction. DMDT is an organochlorine insecticide that brings skin irritation upon dermal contact. Chronic DMDT exposure can affect the liver, kidneys, nervous, and reproductive systems. FT is used as an insecticide with low toxicity toward humans and mammals but possesses very harmful effects on the environment, especially on birds; thus, it has been disapproved by Food and Drug Administrations in many developed countries. FNT is an inexpensive insecticide used as a selective acaricide against chewing and sucking insects on rice, orchard fruits, vegetables, cereals, cotton, and forest. Fenitrothion is toxic to aquatic animals and can cause headaches, drowsiness, dizziness, confusion, blurred vision, slurred speech, convulsions, and depression in human beings. RL is an insecticide that causes skin infection, nausea, weakness, blurred vision, and serpiginous ulcers upon prolonged use.

The mentioned POPS can be transported via wind and water and can affect human beings, animals as well as aquatic species around the world even if they are used in limited regions. Even though the use of POPs is banned in agriculture and various other sectors across the world, various ignorant groups still use them to control pests, to prevent crops from disease, and to improve agriculture production, being unaware of their serious consequences.[5] Moreover, in many lands where POPs are not used for years, they can still be present at a quantifiable concentration as their half-life periods are expected to be nearly two to fifteen years in the soil[6] and even in water. As most of the POPs are highly hydrophobic, the soil is considered the major sink/source with traces of POPs.[7] Since POPs are present in very low quantities, it is crucial to detect them with enhanced sensitivity in various environmental contaminations like water, food and mostly in soil[8] medium. So far, various advanced oxidation technologies (AOTs) and Photocatalysis methods are being used to eliminate POP$_S$ from the environment. However, their detection at lower concentrations is still a serious issue.[9] Several metal–organic frameworks (MOFs) are investigated for detecting organophosphate pesticide detection but with a limitation at low detection limit.[10]

Due to their unique chemical and physical properties, 2D materials are the most attractive option for ultrasensitive and selective sensing of harmful and toxic chemicals,[11-13] gases,[14,15] microorganisms, biomolecules,[16] volatile organic compounds for environmental monitoring (VOCs)[17] to healthcare[18] and even the radiations.[19] The current demand is growing exponentially for these easy-to-handle, affordable, low-cost 2D-based sensors, which are compatible with modern fabrication technologies.[20-22] Several 2D materials like graphene, graphene oxide (GO), transition metal dichalcogenides (TMDs),[17] hexagonal boron nitride (h-BN),[23,24] MXenes,[25,26] Phosphorene (BP),[18,27-29] bismuthene,[30] germanene,[31] stanene,[32] and graphdiyne[33] have been widely explored to develop high-performance chemiresistive sensors. The sensing mechanism of 2D materials is adorned with an inherent resistance modulated in the presence or absence of the target molecules.[34]

Carbon-based 2D materials are the dominating candidates in many sensor applications because of their porosity, high carrier mobility, and excellent electrical and thermal conductivities.[35] Further, the nitrogen content in the carbon-based structures opens a new avenue for metal-free carbon-based nanomaterials in gas sensing applications.[36] For example, graphitic carbon nitrides (g-C_3N_4) with multiple C−N hybridizations (sp, sp^2, and sp^3) have been widely investigated as gas-sensing material.[37,38] Various other carbon nitride systems have been investigated as sensing materials for pollutants in water and soil,[39-41] though with several limitations on lower detection limits. By changing the C−N ratio, a promising 2D material, C_3N_5, has recently been synthesized, possessing high photocatalytic activity.[42,43] The small bandgap (2.27 eV) of C_3N_5 has also been reported to have high adsorption efficiency toward CO_2 gas molecules.[44,45]

Despite promising properties, most of the 2D materials have been least investigated for selective sensing of POPs. To bridge this gap, we used first-principles calculations based on density functional theory (DFT) to study the ground-state structures, electronic properties, and gas-sensing features of C_3N_5 monolayers toward five representative POPs, such as DDT, DMDT, FT, FNT, and RL. Our results reveal that POPs alter the electronic properties of C_3N_5, which is an important parameter for efficient sensing.

2. Methodology

In this work, we employed density functional theory (DFT) calculations as implemented in the VASP package.[46-48] The projected augmented wave (PAW) method with generalized gradient approximation (GGA), by taking Perdew–Burke–Ernzerhof exchange (PBE), was employed to take care of the exchange and correlation interactions of electrons.[49] The supercell geometry of the C_3N_5 structure was modeled by taking a $2 \times 2 \times 1$ supercell along with a vacuum spacing of 20 Å along perpendicular to the sheet surface (conventional z-direction) as presented in **Figure 1**. To obtain the ground state structures, keeping the supercell volume and geometry fixed, the ionic positions and lattice parameters were allowed to relax without any symmetry constraints using the conjugate gradient (CG) algorithm. For structure optimization, the total residual force acting on each atom of the chosen system was allowed to relax until it converged to 0.01 eV Å^{-1}. The energy difference between two conjugate self-consistency calculations was set to be 10^{-7} eV for the energy convergence. Ground state structures were obtained with the Brillouin zone with a KPOINTS grid of $3 \times 3 \times 1$ within the Monkhorst-pack scheme,[50] whereas for calculating electronic properties of the modeled systems, a denser KPOINTS mesh of ($5 \times 5 \times 1$) was used. The cut-off energy for the plane-wave basis set was considered with an optimized energy of 500 eV. To accurately estimate the adsorption energies of the non-covalently bonded POPs to the host C_3N_5, the van der Waals (vdW) dispersion-corrected DFT-D3 approach proposed by Grimme was considered throughout the calculations.[51]

**ADVANCED
SCIENCE NEWS**

www.advancedsciencenews.com

**ADVANCED
THEORY AND
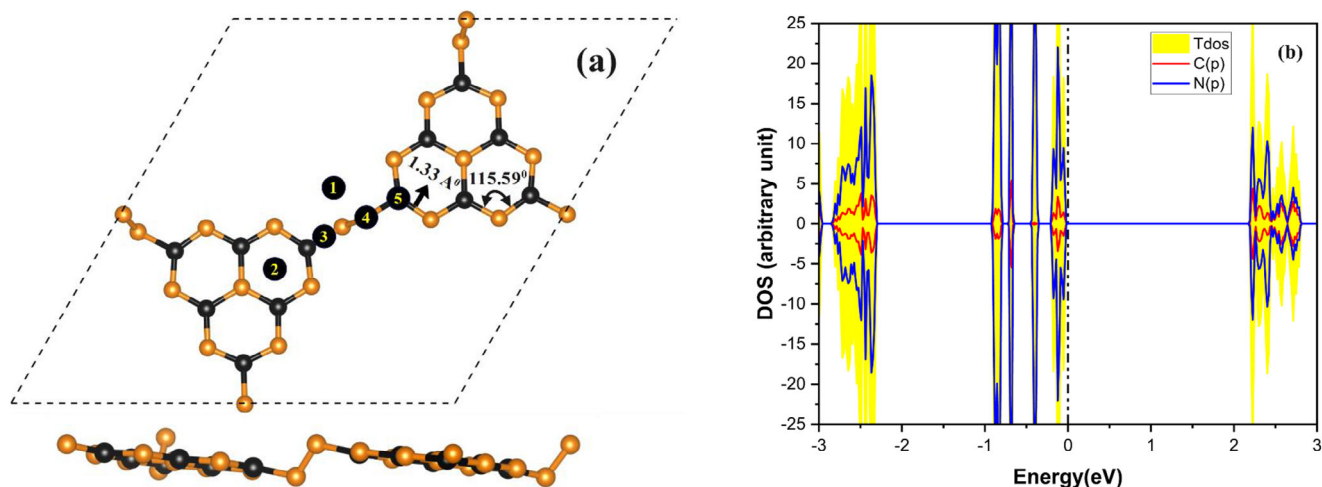SIMULATIONS**

www.advtheorysimul.com

Figure 1. a) The top and side views of the optimized structure of C_3N_5 representing bond distance and bond angles. (Color; Black: Carbon, Orange: Nitrogen). Numbering with black spots are the possible adsorption sites for the considered POPs. b) The total DOS along with C(2p) and N (2p) DOS contribution for the C_3N_5. The dotted vertical line presents the Fermi level.

The adsorption energies (E_{ads}) of the POPs to the C_3N_5 sheet are calculated as,

$$E_{ads} = E_{C3N5-POP} - E_{C3N5} - E_{POP} \tag{1}$$

Here, the first, second and third terms on the right-hand side present the total energies of C_3N_5 adsorbed with the POPs, bare C_3N_5 and POPs, respectively.

Further, the planner average of the electrostatic potential $V_{(xyz)}$ on a real space grid that is averaged over the surface of (surface normal is along the conventional z-axis) C_3N_5 can be calculated as,

$$\overline{V_z} = \frac{1}{A} \iint_{cell} V(x, y, z) \, d_x d_y d_z \tag{2}$$

Here, A presents the area of the modeled C_3N_5 sheet. While plotting $\overline{V_z}$ as a function of z, one can extract the electrostatic potential in a vacuum as $\overline{V_\infty}$. Further, the surface work function (ϕ), which is the minimum energy essential to remove the electron from the surface to the vacuum, is estimated as;

$$\phi = V_\infty - E_f \tag{3}$$

Here, V_∞ and E_f are the electrostatic potential at the point far from the target surface (vacuum) and at the Fermi level of the modeled system, respectively.

To calculate the energetics of solute-solvent interaction with water as a continuous medium surrounding the C_3N_5 and POPs, the implicit solvation method (ISM), as implemented in the VASP code,[52] has been used . The specific dielectric constant of water solvent and its corresponding reaction barriers on the POPs and surfaces of C_3N_5 were utilized to calculate the effects of water on the corresponding adsorption energies.

Taking water as the solvent, the adsorption energy E_{AQad} can be estimated as,

$$E_{AQad} = E_{(C3N5-POP)aq} - E_{(C3N5)aq} - E_{(POP)aq} \tag{4}$$

The first, second, and third terms present the total energies in an aqueous medium for C_3N_5-POPs, C_3N_5 and the POP molecules, respectively.

The solvation energy in the water medium is being estimated as.

$$E_{sol} = E_{vac} - E_{aq} \tag{5}$$

The first and second terms in the equation present the total energy of any system calculated in vacuum and solution (in this case, water) medium, respectively.

3. Results and Discussion

We start with the ground-state structures and the corresponding electronic properties of C_3N_5, as presented in Figure 1a,b. The optimized C—C and C—N bond lengths and C—C—C and C—N—C bond angles are calculated to be 1.34 A° and 116.25°, as mentioned in Figure 1a. SPDOS reveals a non-magnetic character of C_3N_5 with a bandgap of 2.27 eV. The calculated bandgap matches well with previously reported results.[53–55]

Next, we explore the most favorable adsorption sites of the POPs on the C_3N_5 by considering all the available binding sites, such as 1) big-hollow-site, 2) small-hollow-site, 3) C—N bridge, 4) C-top, 5) N-top, as marked in Figure 1a. Further, different orientations of the POPs are considered, and structural optimizations have been performed to obtain the lowest energy configurations. The binding energetics of the adsorbed POPs at the equilibrium configurations are summarized in **Table 1**.

The optimised structures and the corresponding SPDOS of C_3N_5_DDT are presented in **Figures 2**a and **3**a, respectively showing that DDT prefers adsorption on C_3N_5. Upon DDT adsorption, the structure of C_3N_5 gets significantly buckled. The E_{ads} of DDT is calculated as −0.93 eV. Similar to DDT, DMDT, FT, and FNT also prefer parallel orientations over C_3N_5 (Figure 2b–d), resulting into E_{ads} values of −1.55, −1.44, and −0.98 eV, respectively. However, RL prefers tilted orientation and adsorbs on the hollow site (1) of the C_3N_5, as shown in Figure 2e with E_{ads}

ADVANCED
SCIENCE NEWS
www.advancedsciencenews.com

ADVANCED
THEORY AND
SIMULATIONS
www.advtheorysimul.com

Table 1. Binding Energies (E_{ads}), Equilibrium distances of molecules from the corresponding C_3N_5 (R_{eq}), Work function (ϕ), and bandgaps.

System	E_{ads} [eV]	R_{eq} [A⁰]	ϕ [eV]	Bandgap [eV]
C_3N_5		1.34	6.37	2.27
C_3N_5-DDT	−0.93	1.33	3.96	1.20
C_3N_5-DMDT	−1.55	1.33	2.54	1.20
C_3N_5-FNT	−1.44	1.33	5.50	2.00
C_3N_5-FT	−0.98	1.33	4.28	0.80
C_3N_5-RL	−1.15	1.0	3.50	1.70

value of −1.15 eV. The strong E_{ads} values of POPs result in significant structural disintegration of C_3N_5. It has been reported that the surface interaction depends on saturated surface concentration, which could result in a slower response to desorption depending upon the particle sizes.[56,57] The DOS plots show that the adsorption of the studied POPs results in reduced bandgap of C_3N_5, which suggests the formation of chemical bonding between them. The respective PDOS plots also reveal that the hybridized POPs-C_3N_5 states get pushed to the conduction band region.

In the case of C_3N_5-DDT, the bandgap gets reduced to 1.20 eV (Figure 3a) as compared to 2.27 eV, i.e. the bandgap of the bare C_3N_5 system (Figure 1b. DDT optimizes at a distance of 1.33 Å from C_3N_5 (Figure 2a). A significant structural distortion is evident upon DDT adsorption, which implies the sub-lattice symmetry breaking of the host C_3N_5. The adsorption of DDT results

in weak hydrogen bond formation between the DDT and C_3N_5 surface, involving an exothermic reaction with an energy release of −0.90 eV. DDT creates a strong perturbation in the C_3N_5 surface, which modulates the electronic configuration of C_3N_5-DDT, decreasing the bandgap energy.[58] From the Bader charge analysis, it is revealed that upon adsorption of DDT, the carbon atoms of C_3N_5 lose charge of ≈0.7 é and act as a cation. On the other hand, the bigger DDT molecule gains a charge of ≈0.2 é. Overall, there is a charge transfer from sheet i.e. from the electron-deficient C part of the C_3N_5 (**Figure 4**a). The reduced bandgap is solely due to the bond formation between DDT and C_3N_5, where the electronic states from the DDT molecules like Cl-*3p* H-*1s*, strongly hybridize with C-*2p* states in the valence band region lying at the edge of Fermi level whereas, N-*2p* and C-*2p* hybrid states (Figure 3a) are more likely at the edge of conduction band states, which will not contribute to electron conduction.

In the case of C_3N_5-DMDT, comparatively bigger DMDT molecule adsorbs at a distance of 1.33 Å from C_3N_5 (Figure S1, Supporting Information). It prefers to sit flat on the big hollow site with its C and H atoms oriented toward the C_3N_5, as shown in Figure 2b. A significant structural distortion in C_3N_5 is evident upon the adsorption of DMDT (Figure 3b) with a reduced bandgap of 1.20 eV. The SPDOS plot reveals that C-*2p* states of the host C_3N_5 sheet strongly hybridize with O-*2p*, H-*1s* and Cl-*3p* states of the DMDT in the valance band region at the edge of the Fermi level. In contrast, the C-*2p* and N-*2p* hybrid bands in the conduction band region of the host sheets are pushed away, resulting in a reduced bandgap (Figure 3b) compared to the bare C_3N_5 sheet. For the DMDT, the C and H atoms orienting toward
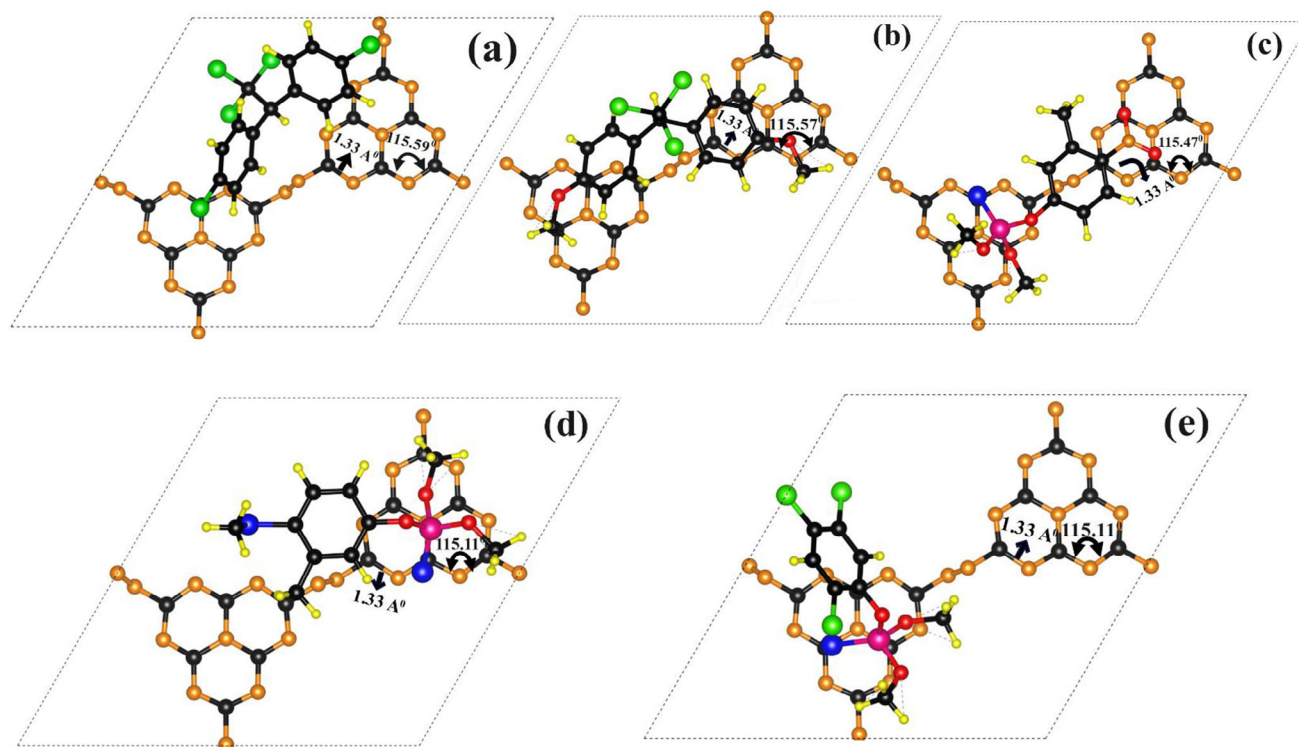

Figure 2. a–e) are the top views of the optimized structures of C_3N_5-DDT, C_3N_5-DMDT, C_3N_5-FNT, C_3N_5-FT, and C3N5-RL, respectively (Color; Black: Carbon, Orange: Nitrogen, Chlorine: Green Yellow: Hydrogen, Red: Oxygen, Navy Blue: Sulphur, Bright Pink: Phosphorus).
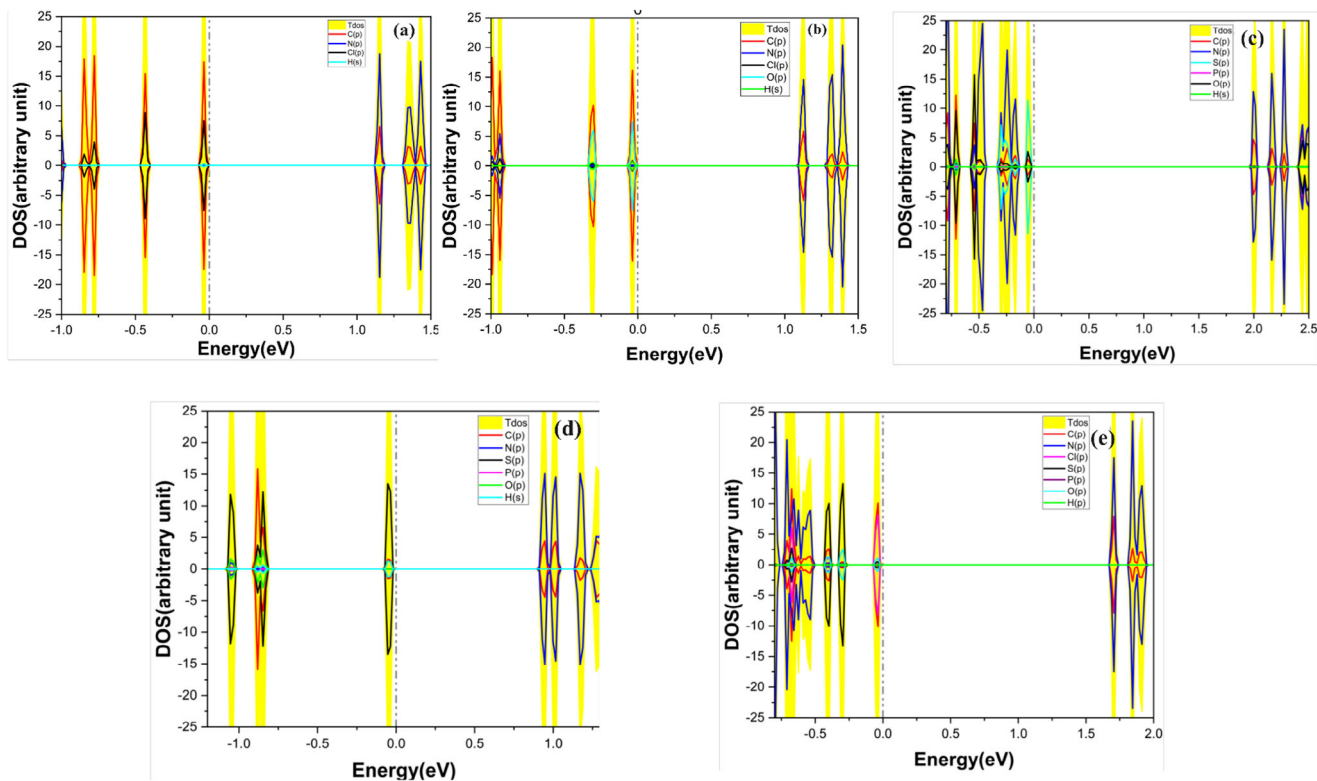
**ADVANCED
SCIENCE NEWS**

www.advancedsciencenews.com

**ADVANCED
THEORY AND
SIMULATIONS**

www.advtheorysimul.com

Figure 3. a–e) are the SPDOS C_3N_5- DDT, C_3N_5-DMDT, C_3N_5-FNT, C_3N_5-FT, and C_3N_5-RL, respectively, and the dotted line presents the Fermi Level (Color; Red: Carbon, Navy Blue: Nitrogen, Harlequin: Chlorine, Yellow: Hydrogen, Aqua: Oxygen, Chocolate: Sulphur, Bright Pink: Phosphorus).
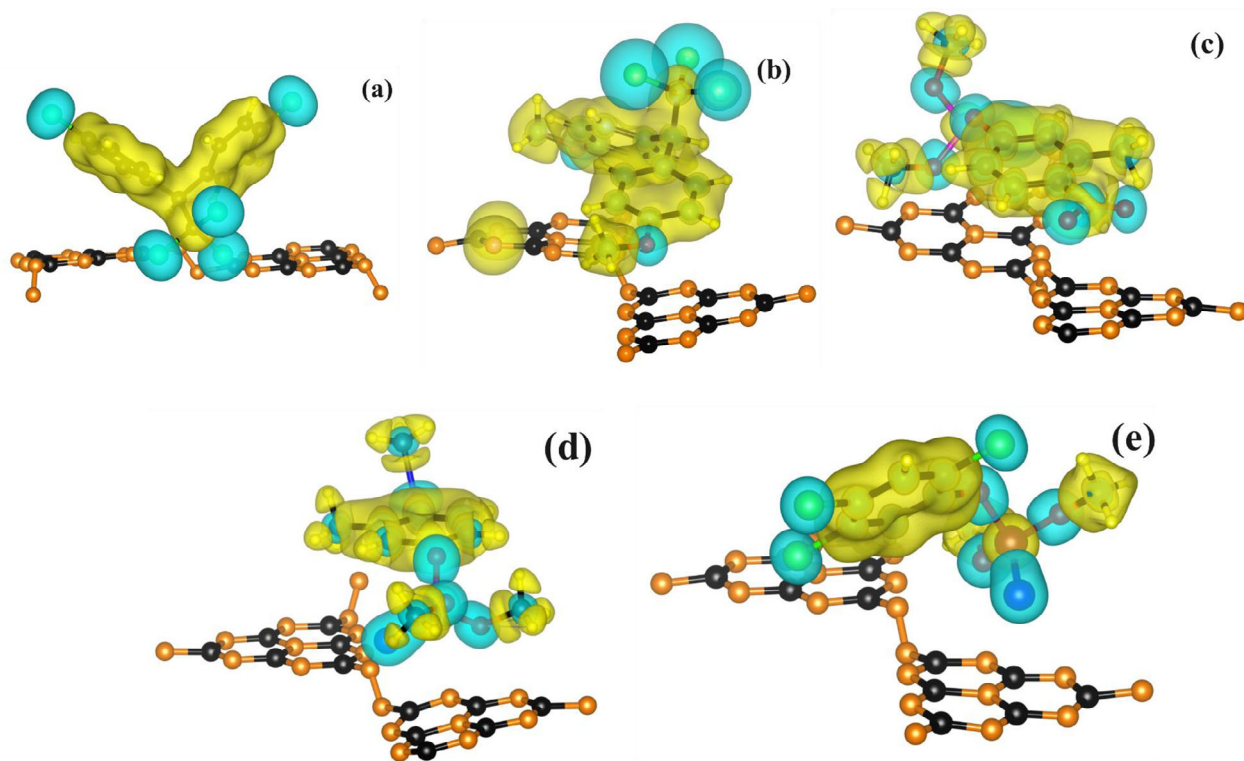

Figure 4. a–e) are the net charge density of C_3N_5-DDT, C_3N_5-DMDT, C_3N_5-FNT, C_3N_5-FT, and C_3N_5-RL, respectively. The yellow and cyan colors represent the charge accumulation and depletion regions, respectively, with iso value 0.005 eÅ^{-3}.

ADVANCED
SCIENCE NEWS

www.advancedsciencenews.com

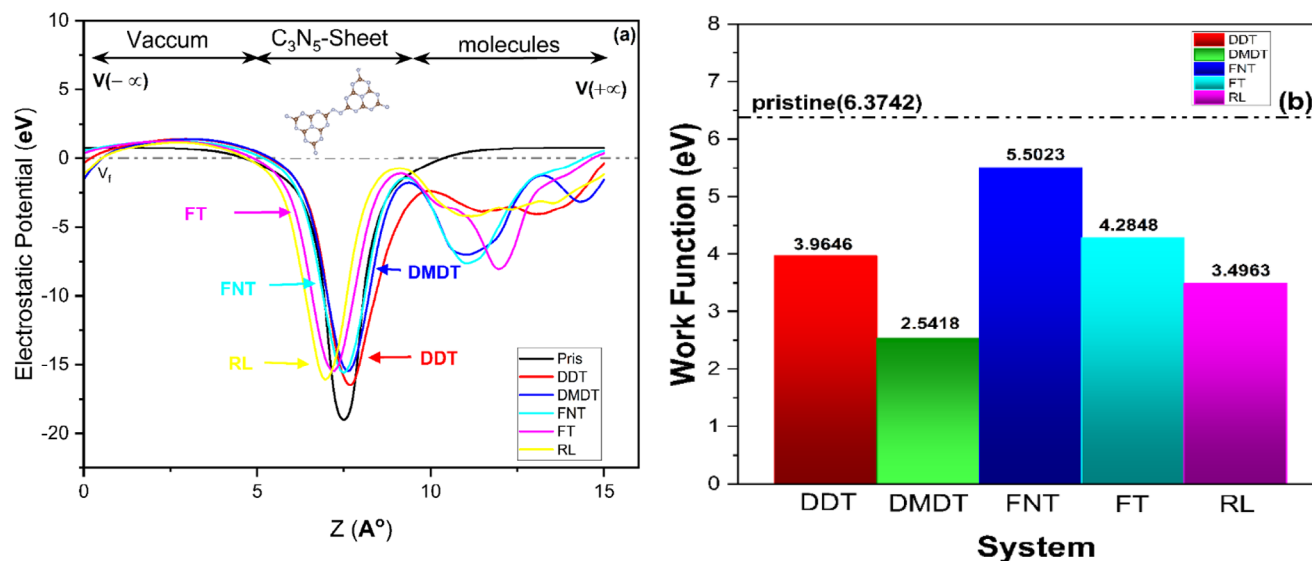**ADVANCED**
THEORY AND
SIMULATIONS

www.advtheorysimul.com

Figure 5. a) calculated the planner average electrostatic potentials (Vz) of C_3N_5 and C_3N_5-POPs. b) Variation in the work function (ϕ) values.

the C_3N_5 lose, whereas the Cl and O atoms gain charges orienting a strong dipole moment (Figure 4b), which results in sturdy binding between C_3N_5 and DMDT.

Similar effects have been observed for C_3N_5-FNT, C_3N_5-FT, and C_3N_5-RL systems, where the FNT, FT, and RL strongly bind and result in significant structural distortion in C_3N_5 (Figure 2c–e). The distortion in lattice symmetry of C_3N_5 also initiates an decrease in its bandgap (Figure 3c–e) to 2.0 eV (C_3N_5-FNT), 0.80 eV (C_3N_5-FT), and 1.7 eV (C_3N_5-RL). The SPDOS plots depicted in Figure 3c–e reveals strong hybridization between the states of the FNT, FT, and RL with C_3N_5 in the valance band region lying at the edge of the Fermi level. The C-2p-N-2p hybrid bands of the host C_3N_5 sheet appear in the conduction band region while reducing the forbidden region for electron conduction. The Bader charge analysis in the case of both C_3N_5-FT and C_3N_5-FNT reveals charge donation from C atoms of C_3N_5. Mostly, the S and O atoms of the adsorbate gain the charge cloud while the P, H and C atoms are on the losing side of the charge cloud (Figure 4c,d). Moreover, the cationic C-site of C_3N_5 acts as the anchoring site to bind the polarized FT and FNT strongly. For the C_3N_5-RL system, the C atom of C_3N_5 loses charge, whereas the Cl, S, and O atoms of RL gain a significant share of that charge (Figure 4e).

3.1. Electrostatic Potential and Work Function

Upon POPs adsorption, redistribution of charges alters the work function and electrostatic potential of C_3N_5, which is

correlated with the variation in the conductance/resistance. The distinct change in the resistance plays a key role in the selective identification of the POPs. To identify the variation in resistance qualitatively, we have calculated the planner average electrostatic potentials (V_z) of bare C_3N_5 and C_3N_5-POPs systems and the results are depicted in **Figure 5**a. With the adsorption of POPs, the V_z of C_3N_5-POPs get strikingly altered at the edge of the Fermi level, V_f. Since the direction of the extra electrostatic field favors the escape of electrons, it indicates the distinct variation in the work function (ϕ) of the corresponding systems. Here, the change in ϕ is calculated for all the C_3N_5-POPs systems to identify selective variation in resistance (Figure 5b). A noteworthy decrease in ϕ of C_3N_5 is evident upon the adsorption POPs. Thus, upon the adsorption of POPs, the bonding interaction induces significant charge redistribution, which contributes to the distinct change in ϕ of C_3N_5-POPs. The ϕ of each C3N5-POP mostly decreases compared to the bare C_3N_5 (**Figure 6**).

3.2. Adsorption Mechanism in Aqueous Medium

Most of the identified POPs are detected in the soil, which will be in moist conditions. Therefore, we have considered the sensing mechanism in the presence of aqueous medium . Taking water as the solvent, the interaction of POPs with C_3N_5 is considered, and the optimized structures and the adsorption energies are shown
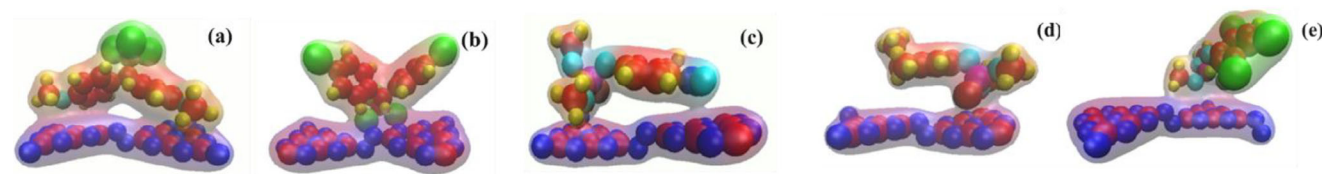

Figure 6. a–e): The optimized structures of a) C_3N_5-DDT, b) C_3N_5-DMDT, c) C_3N_5-FNT, d) C_3N_5-FT, and e) C_3N_5-RL systems in the aqueous environment.

**ADVANCED
SCIENCE NEWS**

www.advancedsciencenews.com

**ADVANCED
THEORY AND
SIMULATIONS**

www.advtheorysimul.com

Table 2. The adsorption energies in aqueous medium (E_{AQad}) and Solvation Energies (E_{sol}).

Systems	E_{AQad}	E_{sol}
C_3N_5		0.60
C_3N_5-DDT	−0.71	1.60
C_3N_5-DMDT	−0.85	2.0
C_3N_5-FNT	−0.92	1.70
C_3N_5-FT	−0.73	1.50
C_3N_5-RL	−0.88	1.40

in Figure 6 (a-e) and in **Table 2**, respectively. It can be seen that the binding energies (E_{AQad}) of the POPs to C_3N_5 decrease. However, the E_{AQad} values are still within the desirable range for a reversible sensing mechanism in the presence of water.

3.3. Thermodynamic Analysis

Because of the large adsorption energies of FNT and DMDT, it is expected that the C_3N_5 substrate will perform effectively when detecting the two gases. Below 100 ppm, a linear relationship between the partial pressure as a gas concentration and surface coverage shows that quantitative sensing is feasible. This result shows lesser performance for RL and somewhat.

The surface coverage of selected pollutant molecules on C_3N_5 as an adsorption performance was estimated based on the Langmuir adsorption model.[59–62] For homogeneous gas, the surface coverage $\theta_X(P, T)$ of target gas molecule X at given partial pressure P_X of and temperature T may be computed by using Equation (6).

$$\theta_X (P, T) = \frac{\exp\left[\left(\mu_X(P, T) - \varepsilon_X\right)/k_B T\right]}{1 + \exp\left[\left(\mu_X(P, T) - \varepsilon_X\right)/k_B T\right]} \tag{6}$$

where $\mu_X(P, T)$ denotes a chemical potential of the surrounding gas and ε_X indicates an adsorption energy obtained by DFT calculation. k_B is the Boltzmann constant. The chemical potentials of selected pollutant molecules were computed by thermochemistry calculation implemented in Gaussian09 software,[62] in ωB97XD/aug-cc-pVTZ[1] level of theory. It was known that these theoretical estimations of the chemical potential of polyatomic gas correspond well to real gas data.[60–62]

Table 3. Fitting parameters in Equation X2. These values are applicable for pressures <1 bar and temperatures ranging from 200 to 700 K. For all these polynomial regressions, the coefficient of determination R^2 is 0.9999.

Pollutant Gas	C_0 [eV]	C_1 [meV K^{-1}]	C_2 [μeV K^{-2}]
DDT	0.05383	−1.60950	−3.89090
DMDT	0.07863	−1.76728	−4.86880
FNT	0.04229	−1.46242	−3.41460
FT	0.04231	−1.50128	−3.51010
RL	0.06634	−1.52941	−3.15560

The calculated chemical potential was formulated as Equation (7) by polynomial regression.

$$\mu_X (P, T) = k_B T \ln\left[\frac{P}{k_B T}\left(\frac{2\pi\hbar^2}{M_X k_B T}\right)^{3/2}\right] + \left(C_0 + C_1 T + C_2 T^2\right) \tag{7}$$

where $\hbar$ and M_X are the Planck constant and molar mass, C_0 to C_2 are fitting parameters shown in **Table 3**. The former term originates from the monatomic ideal gas model, and the latter is the correction for polyatomic thermal motions. There is no significant dependence on pressure in the correction term below 1 bar.

Figure 7 shows the pressure-dependent surface coverage of five pollutant species at room temperature. This result suggests that the C_3N_5-based nanosensor with superior sensitivity can detect target chemicals, particularly DDT and DMDT. The quantitative analysis for the two species can be performed at pressures lower than 10^{-4} bar because of the linear relationship between surface coverage and partial pressure of gas. It is projected that the C_3N_5 substrate has a moderate detecting capability for RL compared to DDT and DMDT and a lower sensing performance for FL and DDT.

4. Summary

We performed first-principles calculations based on density functional theory (DFT) to study the sensing properties of carbon nitride (C_3N_5) monolayers toward a series of persistent organic pollutants (POPs), such as Dichlorodiphenyltrichloroethane (DDT), Methoxychlor (DMDT), Fenthion (FT), Fenitrothion (FNT) and Rennol (RL). Our van der Waals corrected energetic analysis revealed highly desirable adsorption energies of −0.93, −1.55, −1.44, −0.98, and −1.15 eV for DDT, DMDT, FT, FNT, and RM, respectively. In order the study the sensing mechanism in moist conditions, we employed a solvation model, which resulted in slightly lower adsorption energies of −0.71, −0.85, −0.92,
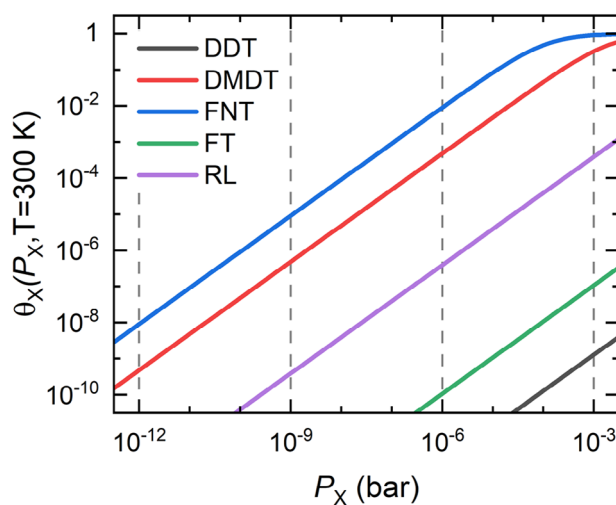

Figure 7. The surface coverage of target organic pollutants on C_3N_5 substrate as a function of partial pressure with fixed temperature at 300 K.

**ADVANCED
SCIENCE NEWS**

www.advancedsciencenews.com

**ADVANCED
THEORY AND
SIMULATIONS**

www.advtheorysimul.com

−0.73, and −0.88 eV for DDT, DMDT, FT, FNT, and RM, respectively. These POPs' adsorption is associated with the transfer of charges, which changes the electronic properties of C_3N_5 monolayers. Variations in the electronic structures of C_3N_5 monolayers upon the adsorption of POPs were studied by means of density of states, electrostatic potential and work function calculations. Langmuir adsorption model was employed to study the sensing mechanism of POPs on C_3N_5 at different temperature and pressure conditions. In conclusion, C_3N_5 monolayers were efficient nanosensors for precisely detecting harmful POPs in both air and aqueous mediums.

Conflict of Interest

The authors declare no conflict of interest.

Data Availability Statement

The data that support the findings of this study are available from the corresponding author upon reasonable request.

[1] G. Burleson, *Fundam. Appl. Toxicol.* **1996**, *29*, 40.
[2] B. E. Erickson, "Linking pollution and infectious disease," c&EN, **2019**, *97*, 28.
[3] C. Heilmann, P. Grandjean, P. Weihe, F. Nielsen, E. Budtz-Jørgensen, *PLoS Med.* **2006**, *3*, e311.
[4] H. PO. Tang, *TrAC – Trends Anal. Chem.* **2013**, *45*, 48..
[5] EPA, "Persistent Organic Pollutants: A Global Issue, A Global Response," United states Environmental Protection Agency, https://www.epa.gov/international-cooperation/persistent-organic-pollutants-global-issue-global-response#top, (accessed: January 2002).
[6] M. A. Ashraf, *Environ. Sci. Pollut. Res.* **2017**, *24*, 4223.
[7] F. Caroleo, G. Magna, M. L. Naitana, L. Di. Zazzo, R. Martini, F. Pizzoli, M. Muduganti, *Environ. Monit.* **2022**, *22*, 2649.
[8] N. Gaur, D. Dutta, A. Singh, R. Dubey, D. V. Kamboj, *Front. Environ. Sci.* **2022**, *10*, 872514.
[9] E. Mahmoudi, H. Fakhri, A. Hajian, A. Afkhami, H. Bagheri, *Bioelectrochemistry* **2019**, *130*, 107348.
[10] P. Panigrahi, T. Hussain, A. Karton, R. Ahuja, *ACS Sens.* **2019**, *4*, 2646.
[11] P. Panigrahi, D. Jini, H. Bae, H. Lee, R. Ahuja, T. Hussain, *Appl. Surf. Sci.* **2021**, *542*, 148590.
[12] M. Sagynbaeva, T. Hussain, P. Panigrahi, B. Johansson, R. Ahuja, *EPL* **2015**, *109*, 57008.
[13] G. S. Rao, T. Hussain, M. S. Islam, M. Sagynbaeva, D. Gupta, P. Panigrahi, R. Ahuja, *Nanotechnology* **2015**, *27*, 015502.
[14] T. Hussain, P. Panigrahi, R. Ahuja, *Phys. Chem. Chem. Phys.* **2014**, *16*, 8100.
[15] T. Hussain, P. Panigrahi, R. Ahuja, *Nanotechnology* **2014**, *25*, 325501.
[16] P. Panigrahi, Y. Pal, D. Raval, S. K. Gupta, P. N. Gajjar, H. Bae, H. Lee, S. Mark, R. Ahuja, R. Pandey, T. Hussain, *Mater. Today Chem.* **2022**, *26*, 101069.
[17] P. Panigrahi, Y. Pal, A. Panigrahi, H. Bae, H. Lee, R. Ahuja, T. Hussain, *Adv. Theory Simul.* **2022**, *5*, 2200357.
[18] P. Panigrahi, M. Sajjad, D. Singh, T. Hussain, J. Andreas Larsson, R. Ahuja, N. Singh, *Appl. Surf. Sci.* **2022**, *573*, 151579.
[19] M. V. Sulleiro, A. Dominguez-Alfaro, N. Alegret, A. Silvestri, I. J. Gómez, *Sens. Bio-Sens. Res.* **2022**, *38*, 100540.
[20] C. Dai, Y. Liu, D. Wei, *Chem. Rev.* **2022**, *122*, 10319.
[21] D. Tyagi, H. Wang, W. Huang, L. Hu, Y. Tang, Z. Guo, Z. Ouyang, H. Zhang, *Nanoscale* **2020**, *12*, 3535.
[22] M. T. Ahmed, S. Hasan, S. Islam, F. Ahmed, *Appl. Surf. Sci.* **2023**, *623*, 157083.
[23] H. Bae, T. Hussain, H. Choi, H. Lee, *Adv. Theory Simul.* **2022**, *5*, 2100409.
[24] P. Panigrahi, Y. Pal, T. Kaewmaraya, H. Bae, N. Nasiri, T. Hussain, *ACS Appl. Nano Mater.* **2023**, *6*, 8404.
[25] H. Vovusha, R. G. Amorim, H. Bae, S. Lee, T. Hussain, H. Lee, *Mater. Today Chem.* **2023**, *30*, 101543.
[26] T. Kaewmaraya, L. Ngamwongwan, P. Moontragoon, W. Jarernboon, D. Singh, R. Ahuja, A. Karton, T. Hussain, *J. Hazard. Mater.* **2021**, *401*, 123340.
[27] S. Sun, T. Hussain, W. Zhang, A. Karton, *Appl. Surf. Sci.* **2019**, *486*, 52.
[28] T. Kaewmaraya, L. Ngamwongwan, P. Moontragoon, A. Karton, T. Hussain, *J. Phys. Chem. C* **2018**, *122*, 20186.
[29] P. Panigrahi, P. K. Panda, Y. Pal, H. Bae, H. Lee, R. Ahuja, T. Hussain, *ACS Appl. Nano Mater.* **2022**, *5*, 2984.
[30] T. Hussain, T. Kaewmaraya, S. Chakraborty, H. Vovusha, V. Amornkitbamrung, R. Ahuja, *ACS Sens.* **2018**, *3*, 867.
[31] H. Vovusha, T. Hussain, M. Sajjad, H. Lee, A. Karton, R. Ahuja, U. Schwingenschlögl, *Appl. Surf. Sci.* **2019**, *495*, 143622.
[32] S. Singsen, N. Thasami, P. Tangpakonsab, H. Bae, H. Lee, T. Hussain, T. Kaewmaraya, *Phys. Chem. Chem. Phys.* **2022**, *24*, 26622.
[33] R. Khan, A. Radoi, S. Rashid, A. Hayat, A. Vasilescu, S. Andreescu, *Sensors* **2021**, *21*, 3369.
[34] E.-M. Kirchner, T. Hirsch, *Microchim. Acta* **2020**, *187*, 441.
[35] Y. Yong, H. Cui, Q. Zhou, X. Su, Y. Kuang, X. Li, *Appl. Surf. Sci.* **2019**, *487*, 488.
[36] V. S. Bhati, V. Takhar, R. Raliya, M. Kumar, R. Banerjee, *Nano Express* **2022**, *3*, 014003.
[37] P. Srinivasan, S. Samanta, A. Krishnakumar, J. B. B. Rayappan, K. Kailasam, *J. Mater. Chem. A* **2021**, *9*, 10612.
[38] A. Kotbi, M. Benyoussef, E. M. Ressami, M. Lejeune, B. Lakssir, M. Jouiad, *Chemosensors* **2022**, *10*, 470.
[39] P. Noyrod, O. Chailapakul, W. Wonsawat, S. Chuanuwatanakul, *J. Electroanal. Chem.* **2014**, *719*, 54.
[40] S. S. Miao, M. S. Wu, L. Y. Ma, X. J. He, H. Yang, *Talanta* **2016**, *158*, 142.
[41] T. Liu, G. Yang, W. Wang, C. Wang, M. Wang, X. Sun, P. Xu, J. Zhang, *Environ. Res.* **2020**, *188*, 109741.
[42] J. Liu, S. Wang, C. Zhao, J. Zheng, *Nanomaterials* **2023**, *13*, 499.

[43] S. Kim, G. Singh, C.i Sathish, P. Panigrahi, R. Daiyan, X. Lu, Y. Sugi, I. Y. Kim, A. Vinu, *ChemAn Asian J.* **2021**, *16*, 3999.

[44] L. Huang, Z. Liu, W. Chen, D. Cao, A. Zheng, *J. Mater. Chem. A* **2018**, *6*, 7168.

[45] V. Wang, N. Xu, JC. Liu, G. Tang, WT. Geng, *Comput. Phys. Commun.* **2021**, *267*, 108033.

[46] Y. Chen, Y. Yang, C. Xu, H. Xiang, *Phys. Rev. B* **2023**, *107*, 214439.

[47] ZL. Liu, C. E. Ekuma, WQ. Li, JQ. Yang, XJ. Li, *Comput. Phys. Commun.* **2022**, *270*, 108180.

[48] J. P. Perdew, K. Burke, M. Ernzerhof, *Phys. Rev. Lett.* **1996**, *77*, 3865.

[49] S. R. Naqvi, T. Hussain, P. Panigrahi, W. Luo, R. Ahuja, *RSC Adv.* **2017**, *7*, 8598.

[50] S. Grimme, *J. Comput. Chem.* **2006**, *27*, 1787.

[51] P. Panigrahi, Y. Pal, A. Panigrahi, H. Bae, H. Lee, R. Ahuja, T. Hussain, *Adv. Theory Simul.* **2022**, *5*, 2200357.

[52] Z. Cai, Y. Huang, H. Ji, W. Liu, J. Fu, X. Sun, *Sep. Purif. Technol.* **2022**, *280*, 119772.

[53] X. Niu, S. Xiao, Y. Li, C. Quan, D. Sun, J. Ge, Y.u Chen, S. Li, X. '. Li, *Solid State Commun.* **2023**, *371*, 115233.

[54] B. Mortazavi, F. Shojaei, M. Shahrokhi, M. Azizi, T. Rabczuk, A. V. Shapeev, X. Zhuang, *Carbon* **2020**, *167*, 40.

[55] X. Fang, B. Liu, K. Cao, P. Yang, Q. Zhao, F. Jiang, Y. Xu, R. Chen, X. Liu, *ACS Catal.* **2020**, *10*, 2799.

[56] F. Jiang, Y. Yang, L. Wang, Y. Li, Z. Fang, Y. Xu, B. Liu, X. Liu, *Catal. Sci. Technol.* **2022**, *12*, 551.

[57] A. Sahithi, K. Sumithra, *RSC Adv.* **2020**, *10*, 42318.

[58] H. Bae, M. Park, B. Jang, Y. Kang, J. Park, H. Lee, H. Chung, C. Chung, S. Hong, Y. Kwon, B. I. Yakobson, H. Lee, *Sci. Rep.* **2016**, *6*, 21788.

[59] T. Hussain, M. Sajjad, D. Singh, H. Bae, H. Lee, J. A. Larsson, R. Ahuja, A. Karton, *Carbon* **2020**, *163*, 213.

[60] A. Singh, H. Bae, S. Lee, K. Shabbiri, T. Hussain, H. Lee, *Appl. Surf. Sci.* **2020**, *512*, 145641.

[61] S. Singsen, N. Thasami, P. Tangpakonsab, H. Bae, H. Lee, T. Hussain, T. Kaewmaraya, *Phys. Chem. Chem. Phys.* **2022**, *24*, 26622.

[62] JD. Chai, M. Head-Gordon, *J. Chem. Phys.* **2008**, *128*, 84106.

2300697 (9 of 9)